Synthesis of ZnO and SnO_2 catalysts using roselle flower extract for biodiesel production from waste cooking oil

Maisari Utami[1,2*], *Izzaty Fauziya* Salwa[1], and *Marisa*[1]

[1]Department of Chemistry, Faculty of Mathematics and Natural Sciences, Universitas Islam Indonesia, Yogyakarta 55584, Indonesia
[2]Nanomaterials and Sustainable Chemistry Research Centre, Universitas Islam Indonesia, Yogyakarta 55584, Indonesia

Abstract. The development of biodiesel from waste cooking oil using green-synthesized heterogeneous catalysts offers a sustainable alternative to fossil fuels. In this study, ZnO and SnO_2 catalysts were synthesized using roselle flower (*Hibiscus sabdariffa* L.) extract and applied to transesterification. Characterization revealed that SnO_2 exhibited a surface area of 51.52 m^2/g and a pore volume of 0.080 cm^3/g, nearly 12 times higher than ZnO (4.11 m^2/g; 0.009 cm^3/g), resulting in superior catalytic activity. FTIR analysis of biodiesel catalyzed by ZnO showed ester-specific peaks at 1115 cm^{-1} (C–O) and 1022 cm^{-1} (C–O–C), while biodiesel from SnO_2 displayed a strong ester carbonyl band at 1744 cm^{-1}, confirming FAME formation. GC–MS results indicated that ZnO-catalyzed biodiesel consisted mainly of methyl oleate (60.23%), methyl palmitate (34.83%), methyl stearate (2.27%), and methyl myristate (0.34%), with a total FAME content of 97.34%. In contrast, SnO_2-catalyzed biodiesel contained methyl oleate (55.85%), methyl palmitate (37.12%), methyl stearate (4.50%), and methyl myristate (0.64%), yielding nearly 100% FAME. The dominance of methyl oleate and palmitate confirmed the production of high-quality biodiesel with balanced oxidative stability and combustion properties. Therefore, roselle-extract-based SnO_2 demonstrated greater potential than ZnO as an eco-friendly catalyst for biodiesel production from waste cooking oil.

1 Introduction

Currently, the use of cleaner and more sustainable energy is a global focus due to the depletion of fossil fuel resources, global warming, and rising energy costs [1]. The development of abundant and environmentally friendly energy sources is a key solution to climate change, energy security, and economic stability. Biodiesel, derived from vegetable oils or animal fats, is a promising renewable fuel that can be used directly in diesel engines and is environmentally friendly, biodegradable, and low in toxicity.

* Corresponding author: maisariutami@uii.ac.id

Recent studies highlight biodiesel from waste cooking oil (WCO) as a potential circular economy approach to reduce greenhouse gas emissions and valorize waste [2].

Transesterification is a catalytic process in which triglycerides from animal fats or vegetable oils react with alcohols, typically methanol, to yield methyl esters as the primary product and glycerol as a by-product [3]. Transesterification, also referred to as alcoholysis, is a dissociation process analogous to hydrolysis, in which one alcohol is substituted by another within an ester molecule [4]. The reaction rate is mainly influenced by temperature, reaction time, catalyst, and alcohol concentration. Typically, it is carried out at 30–65 °C, near the boiling point of methanol, where higher temperatures shorten reaction time while lower temperatures may improve conversion efficiency [5].

In the transesterification process, catalysts play a crucial role in accelerating the reaction and increasing conversion efficiency. Catalysts can be homogeneous, such as NaOH and KOH, or heterogeneous, such as CaO, ZnO, and SnO_2. Heterogeneous catalysts offer several advantages, including easier separation from the product, reusability, and improved environmental compatibility. ZnO and SnO_2 are increasingly employed due to their stability, high catalytic activity, and resistance to fouling. Mechanistically, metal oxide catalysts function as base sites that accelerate the breakdown of triglycerides into methyl esters and glycerol [6]. For instance, a SnO_2 catalyst impregnated with ZnO nanowires can achieve FAME conversions of up to 92% and can be reused up to five times without regeneration [7].

Green synthesis approaches using plant extracts as reducing agents and stabilizers in catalyst synthesis have received increasing attention, as bioactive plant compounds, such as flavonoids, phenols, and anthocyanins, can facilitate the formation of uniform and catalytically active materials [8]. One potential candidate is the roselle flower (*Hibiscus sabdariffa* L.), which is rich in bioactive compounds and has proven effective as a reducing agent in the synthesis of ZnO and SnO_2 catalysts [9].

Although numerous studies have employed metal oxide catalysts, few have utilized roselle flower extract for WCO-based biodiesel production. Therefore, this study aims to evaluate the effectiveness of roselle extract-based ZnO and SnO_2 catalysts in producing biodiesel from WCO, compare the methyl ester yields obtained from each catalyst, and determine the optimal reaction conditions for maximum conversion.

2 Materials and Methods

2.1 Materials

The materials used in this research were methanol p.a (CH_3OH) from Merck, waste cooking oil, the precursor $SnCl_2.H_2O$ (Tin (II) chloride monohydrate) branded as stannous chloride dihydrate, the precursor $ZnO(NO_2)_3.6H_2O$ (Zinc nitrat hexahydrate) branded as, and filter paper.

2.2 Extraction of Roselle Flower (*Hibiscus sabdariffa* L.)

The ground dried roselle flowers were weighed according to the catalyst requirements, namely 1 g for ZnO and 8 g for SnO_2. Each sample was then dissolved in 100 mL of deionized water and continuously stirred for 1 hour at 60°C to extract the active compounds that function as a bioreducing agent. After the extraction process was complete, the solution was filtered to remove the solids, yielding a clear roselle extract ready to be used in the catalyst synthesis stage.

2.3 Synthesis of Tin (IV) Oxide (SnO_2) Material

The hydrothermal synthesis of SnO_2 was initiated by weighing 0.021 g of $SnCl_2 \cdot 2H_2O$ and dissolving it in 100 mL of distilled water, followed by the addition of 50 mL of roselle flower extract. The mixture was heated at 60 °C for 4 hours under continuous stirring with a magnetic stirrer. The obtained solution was subsequently transferred into an autoclave and maintained at 60 °C for 12 hours. After the reaction, the mixture was filtered to separate the precipitate from the filtrate. The precipitate was collected, placed in a crucible, and oven-dried at 60 °C until completely dry, then calcined at 400 °C for 2 hours in a furnace. Finally, the resulting SnO_2 material was ground into a fine powder and stored in a sealed container. The final product was designated as SnO_2.

2.4 Synthesis of Zinc Oxide (ZnO) Material

The synthesis of ZnO material was carried out by dissolving 2 g of Zn $(NO_3)_2 \cdot 6H_2O$ in 42 mL of roselle extract. The solution was stirred with a magnetic stirrer at 60 °C for 1 hour until completely dissolved, followed by heating in a water bath at the same temperature until it formed a paste-like consistency. The obtained sample was then oven-dried at 60 °C until fully dry. Finally, the dried sample was calcined at 400 °C for 1 hour and subsequently ground into a fine white powder.

2.5 Biodiesel Production Process

In the biodiesel production process, 10 mL of waste cooking oil was first prepared and then mixed with 100 mL of analytical-grade methanol and 0.2 g of metal oxide catalyst (SnO_2/ZnO). The mixture was transferred into a reactor, and the reaction was carried out at 60 °C for 2 hours under continuous stirring with a magnetic stirrer. After completion of the reaction, the mixture was separated using a separatory funnel to divide the upper and lower layers. The upper layer was subsequently filtered using standard filter paper to remove residual catalyst, yielding a purer biodiesel product

3 Results and Discussion

3.1 Materials Characterization

3.1.1 Fourier transmission-infrared spectroscopy (FT-IR)

Fourier Transform Infrared (FTIR) spectroscopy is a technique used to identify the functional groups present in a compound. FTIR works by measuring molecular vibrations and rotations that are influenced by infrared radiation at specific wavelengths. The FTIR results for ZnO show a broad band at 3427 cm^{-1} (O–H stretching) and 1630 cm^{-1} (H–O–H bending), indicating the presence of hydroxyl groups and adsorbed water molecules, along with additional bands at 1385 cm^{-1} (carbonate C-O), 1116 cm^{-1} (C–O), and 870 cm^{-1} (=C–H), which suggest organic residues from the synthesis process (Figure 1). A characteristic band at 514 cm^{-1} confirms the presence of Zn–O bonds, consistent with the theoretical lattice vibration range of Zn–O (430–520 cm^{-1}) reported in the literature [10]. For SnO_2, the spectrum exhibits an O–H band at 3434 cm^{-1} and an H–O–H bending band at 1637 cm^{-1}, followed by a band at 1081 cm^{-1} associated with Sn–OH or C–O, as well as an intense band

at 561 cm^{-1} characteristic of Sn–O vibrations, in agreement with the theoretical range of Sn–O bonds at 550–630 cm^{-1} [11].

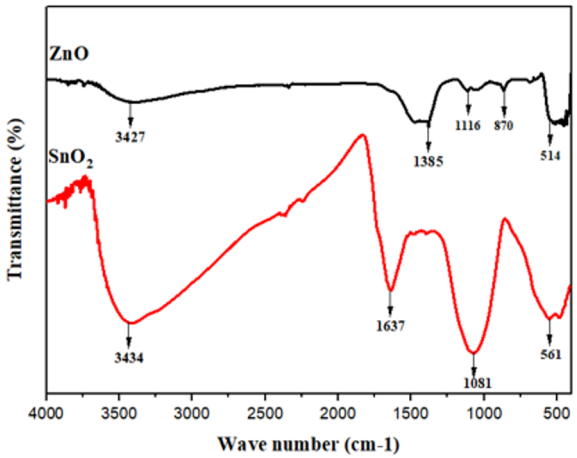

Fig. 1. FTIR spectra of ZnO dan SnO_2.

3.1.2 X-Ray Diffraction (XRD)

X-ray Diffraction (XRD) is a fundamental technique used to identify the crystal structure of materials by analyzing their diffraction patterns. The main parameters such as diffraction angle (2θ), Miller indices (hkl), full width at half maximum (FWHM), and d-spacing are important to determine the crystal phase, degree of crystallinity, and crystallite size. When X-rays strike a material, they are diffracted by the atoms within it. Each crystalline material produces a unique diffraction pattern, much like a fingerprint. The resulting pattern can be compared with a standard crystal pattern database, commonly referred to as JCPDS (Joint Committee on Powder Diffraction Standards). Good crystallinity is indicated by sharp peaks, where the sharper the peaks, the better the crystallinity of the material.

For synthesized SnO_2, the diffraction peaks correspond to the tetragonal rutile phase with JCPDS card no. 41-1445. The most intense diffraction peak is observed at 2θ = 26.589° on the (110) plane with an FWHM of 0.127, confirming strong preferential orientation and good crystallinity. Additional peaks are observed at (101) at 33.888° (FWHM 0.391), (201) at 40.508° (FWHM 0.158), and (211) at 52.704° (FWHM 0.467) (Figure 2). Narrow FWHM values, especially at (110) and (201), indicate larger crystallite size and higher crystallinity, whereas broader FWHM values at (101) and (211) suggest smaller crystallites or strain within the lattice. These findings are in line with Liu et al. (2022), who reported that hydrothermal SnO_2 typically shows a dominant (110) reflection with narrow FWHM, while the (211) peak often appears broader due to heterogeneous crystallite size distribution [12].

Meanwhile, ZnO is identified as a hexagonal wurtzite structure with JCPDS card no. 36-1451. Its diffraction peaks are observed at (100), (002), (101), and higher planes with FWHM values ranging between 0.236-0.387. For instance, at 2θ = 31.68° (hkl 100) with FWHM 0.236, the crystallite size is calculated to be 34.91 nm. At higher angles such as 68.98° with FWHM 0.387, the crystallite size decreases to 24.87 nm. The average crystallite size of ZnO is about 29.04 nm, consistent with nanoscale dimensions and high crystallinity. This result agrees with Zhang et al. (2023), who reported crystallite sizes of 25–35 nm for modified ZnO nanostructures [13].

Comparatively, SnO_2 exhibits its strongest diffraction peak at the (110) plane with a sharp and narrow FWHM, while ZnO shows multiple characteristic peaks (100, 002, 101) with relatively larger average crystallite sizes. This indicates that SnO_2 may have smaller crystallites on certain planes but stronger preferential orientation, whereas ZnO has more uniform crystallinity. Such differences in crystallite size and crystallographic orientation significantly influence the optical absorption and photocatalytic activity of both materials.

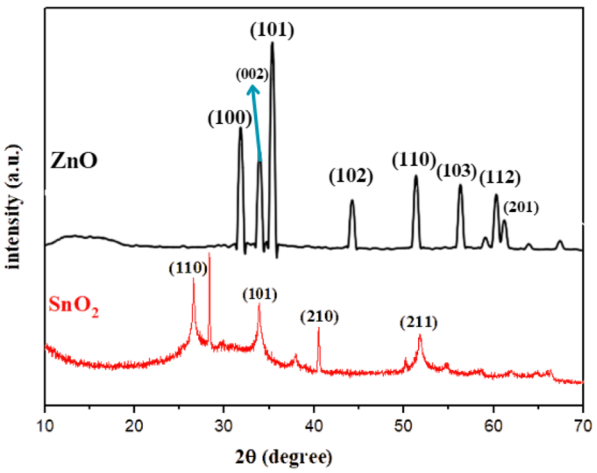

Fig. 2. XRD diffactogram of ZnO and SnO_2.

3.1.3 Gas Sorption Analysis (GSA)

Gas sorption analysis (GSA) is used to determine the surface area, pore volume, and pore size of a material. The analysis is carried out by measuring the amount of gas adsorbed onto the surface of a solid at specific pressures and temperatures [14]. The Brunauer Emmett Teller (BET) equation is used to determine the specific surface area of a material based on gas adsorption data. In its application, the volume of gas adsorbed at various relative pressures is analyzed to obtain the monolayer adsorption capacity (*Vm*), which represents the amount of gas molecules covering the material surface in a single layer. This *Vm* value is then used as the basis for calculating the specific surface area of the material, reflecting the number of active sites available on the surface.

BET equation:

$$\frac{1}{V\left(\frac{P_0}{P}-1\right)} = \frac{C-1}{V_m C}\left(\frac{P}{P_0}\right) + \frac{1}{V_m C} \quad (1)$$

where:

V is the volume of gas adsorbed at a given pressure,

P is the gas pressure,

P_0 is the saturation vapor pressure of the gas,

V_m is the monolayer adsorption capacity, and

C is the BET constant related to the interaction energy between the adsorbed gas and the material surface.

Three types of gases are commonly used in the analysis: helium for micropores (<2 nm), nitrogen for mesopores (2–5 nm), and argon for macropores (>5 nm). The results showed that ZnO exhibited a specific surface area of 4.11 m^2/g, pore volume of 0.00924 cm^3/g, and an average pore size of 2.13 nm. This relatively low surface area suggests that ZnO tends to

agglomerate and possesses a dense morphology with limited porosity, resulting in fewer available active sites and reduced photocatalytic and adsorption activity. In contrast, SnO_2 demonstrated significantly better textural properties with a specific surface area of 51.52 m^2/g, pore volume of 0.08015 cm^3/g, and an average pore size of 3.12 nm (Figure 3 and Table 1). This value is nearly twelve times higher than that of ZnO, indicating the presence of a mesoporous structure that facilitates easier molecular access to active sites and enhances both catalytic and adsorption performance.

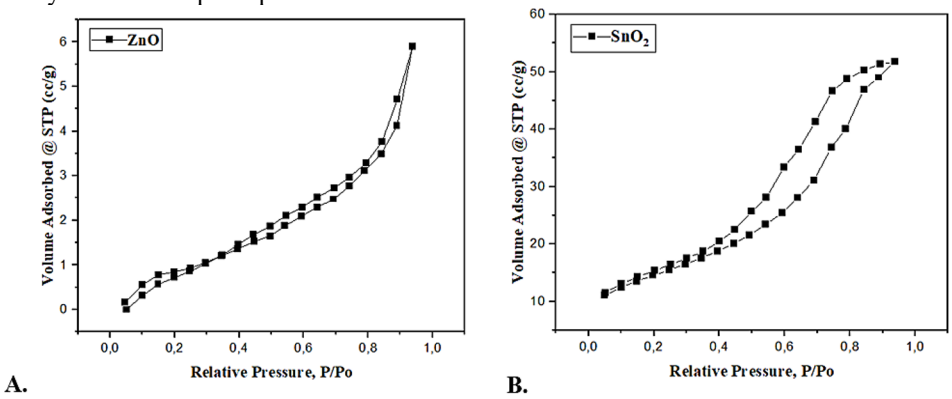

Fig. 3. The adsorption and desorption isotherm curves from the GSA (a) ZnO and (b) SnO_2.

In conclusion, the GSA results highlight a stark contrast between ZnO and SnO_2. ZnO shows low surface area and limited porosity, far below the values reported in recent studies, making it less suitable for photocatalytic applications unless further synthesis optimization is carried out. In contrast, SnO_2 exhibits higher surface area and mesoporosity, aligning well with recent literature, thus offering superior potential for photocatalysis and adsorption applications compared to ZnO.

Table 1. The quantitative GSA results of ZnO and SnO_2.

Description	ZnO	SnO_2
Specific surface area (BET)	4.10952 m^2/g	51.5183 m^2/g
Total pore volume	0.00924157 cm^3/g	0.080153 cm^3/g
Average pore size	2.12638 nm	3.11782 nm

3.1.4 Scanning Electron Microscopy-Energy Dispersive X-ray Spectroscopy (SEM-EDS)

Scanning Electron Microscopy-Energy Dispersive X-ray Spectroscopy (SEM-EDS) is a crucial characterization technique that provides comprehensive information on both the surface morphology and the elemental composition of a material. SEM generates high-resolution images through the interaction of an electron beam with the sample surface, enabling the observation of particle shape, size, and distribution [15]. The combination of these techniques is essential for evaluating the success of inorganic material synthesis, such as ZnO and SnO_2, in terms of both morphological uniformity and elemental purity.

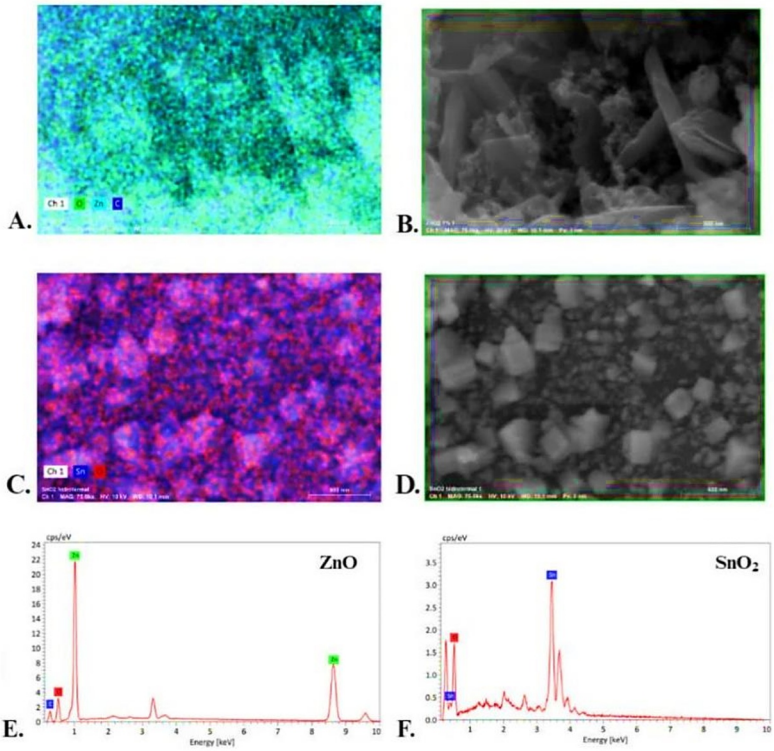

Fig. 4. (a) EDS ZnO elemental mapping, (b) SEM image ZnO, (c) EDS SnO_2 elemental mapping, (d) SEM image SnO_2, EDS spectra of (e) ZnO, and (f) SnO_2.

The characterization results for ZnO reveal that elemental mapping (Figure 4A) shows a homogeneous distribution of Zn and O, indicating the uniform formation of the ZnO phase across the material surface. The SEM image (Figure 4B) demonstrates a morphology dominated by rod-like structures and irregularly shaped particles that tend to agglomerate, which is typically associated with the anisotropic growth behavior of ZnO crystals. The corresponding EDS spectrum (Figure 4E) confirms the presence of Zn and O with mass compositions of 59.05% and 9.48%, respectively. A minor carbon peak was also detected, which is most likely attributed to the conductive carbon coating used during SEM sample preparation rather than being part of the actual ZnO composition.

For SnO_2, elemental mapping (Figure 4C) shows a uniform distribution of Sn and O without significant contamination from other elements, suggesting the successful formation of the SnO_2 phase. The SEM micrograph (Figure 4D) reveals cube-like particles with relatively uniform sizes and dense distributions, indicating a more isotropic crystal growth compared to ZnO. The EDS spectrum of SnO_2 (Figure 4) exhibits dominant peaks of Sn and O, with mass compositions of 83% and 17%, respectively (Table 2). This ratio closely matches the theoretical stoichiometry of SnO_2 (1:2 ratio of Sn to O), thereby confirming the high purity of the synthesized material.

Table 2. Elemental composition of ZnO and SnO_2.

Sample	Mass Concentration (%)		
	Zn	**Sn**	**O**
ZnO	59.05	-	9.48
SnO_2	-	83.00	17.00

Overall, the SEM-EDS analysis demonstrates that both ZnO and SnO_2 were successfully synthesized with distinctive morphologies, homogeneous elemental distributions, and mass ratios consistent with theoretical values. The morphological differences ZnO exhibiting rod-like structures and SnO_2 displaying cube-like particles can be attributed to differences in crystal growth mechanisms and synthesis conditions. Furthermore, the elemental composition results reinforce the effectiveness of the applied synthesis method in producing high-quality ZnO and SnO_2 materials. These findings suggest that the synthesized materials hold significant potential for applications in various fields, particularly as photocatalysts for clean energy reactions and wastewater treatment.

3.2 Biodiesel

The biodiesel synthesis proceeded via a transesterification reaction between triglycerides and methanol using SnO_2 and ZnO as heterogeneous catalysts under mild thermal conditions (60 °C) without light irradiation (Figure 5). SnO_2 and ZnO functioned as solid acid–base catalysts, where Lewis acidic sites (Sn^{4+} and Zn^{2+}) facilitated the activation of the carbonyl (C=O) groups of triglycerides, while basic surface oxygen species promoted the adsorption and activation of methanol into reactive methoxide species.

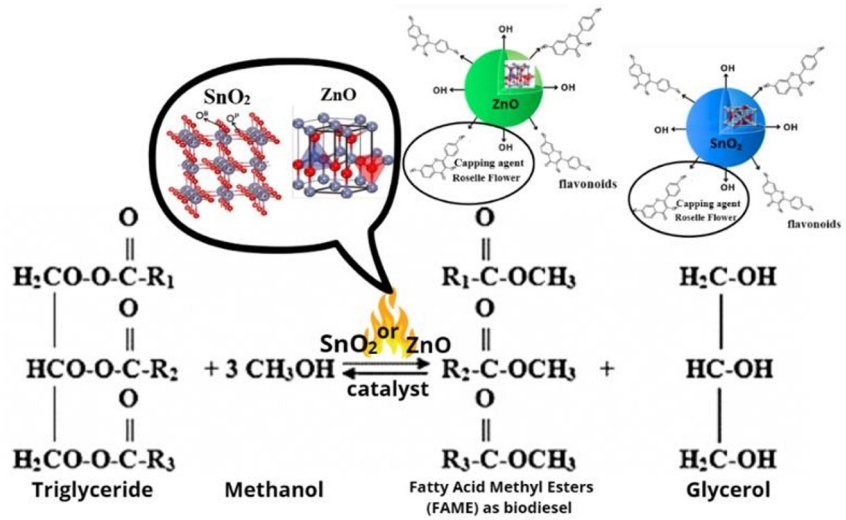

Fig. 5. Illustration of biodiesel production using SnO_2 and ZnO.

The generated methoxide subsequently performed a nucleophilic attack on the electrophilic carbonyl carbon of the triglyceride ester groups, forming tetrahedral intermediates that decomposed into fatty acid methyl esters (FAME) as biodiesel and glycerol as the by-product. The catalytic process was governed solely by thermal energy and catalyst surface interactions, with no involvement of photoinduced electron–hole pairs, confirming the purely heterogeneous catalytic role of SnO_2 and ZnO in the transesterification reaction.

3.3 Biodiesel Characterization

3.3.1 Fourier transmission-infrared spectroscopy (FT-IR)

The FTIR spectrum of ZnO catalyst (Figure 6) shows an absorption peak at 3312 cm^{-1}, which indicates the presence of –OH groups from moisture or residual alcohol, while the bands at

2951 cm^{-1} and 2832 cm^{-1} correspond to asymmetric and symmetric stretching vibrations of C–H from methyl and methylene groups in the aliphatic chain. The absorption at 1451 cm^{-1} indicates C–H bending vibrations, whereas the strong band at 1115 cm^{-1} is related to C–O stretching from ester groups, along with a sharp peak at 1022 cm^{-1} that further confirms the presence of C–O–C bonds in esters, and the band at 630 cm^{-1} is associated with aliphatic C–H bending vibrations, thus confirming that the use of ZnO catalyst produces biodiesel with ester functional group characteristics.

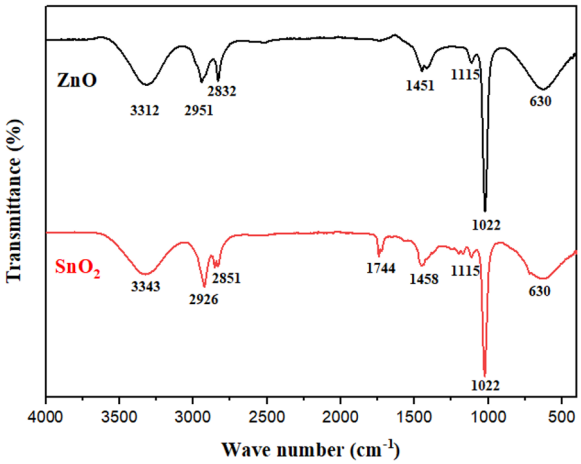

Fig. 6. FTIR spectra results of SnO_2 HT Vis, SnO_2 HT UV, SnO_2 SG Vis, and SnO_2 SG UV.

Meanwhile, the FTIR spectrum of SnO_2 catalyst exhibits an absorption band at 3343 cm^{-1} corresponding to –OH groups, followed by bands at 2926 cm^{-1} and 2851 cm^{-1} indicating C–H stretching vibrations from hydrocarbon chains, as well as a characteristic band at 1744 cm^{-1} that confirms the presence of ester carbonyl (C=O) groups as the main indicator of biodiesel formation. The band at 1458 cm^{-1} is attributed to C–H deformation, while the peaks at 1115 cm^{-1} and 1022 cm^{-1} correspond to C–O stretching vibrations of esters, and the absorption at 630 cm^{-1} is associated with aliphatic C–H bonds, thereby confirming that SnO_2 is also effective in assisting the transesterification process, with the ester carbonyl peak serving as strong evidence for the formation of fatty acid methyl ester biodiesel.

3.3.2 Gas Chromatography–Mass Spectrometry (GC–MS)

Gas Chromatography–Mass Spectrometry (GC–MS) is an analytical technique used to separate, identify, and quantify chemical compounds with high accuracy. GC–MS analysis produces chromatograms showing analyte separation based on retention time and fragmentograms displaying mass fragmentation patterns that provide information on molecular structure.

GC–MS analysis of the catalyst ZnO (Figure 7) without light sample revealed that the biodiesel is dominated by four major compounds with a total content reaching 97.34%. The most abundant compound is methyl oleate (RT 16.836 min, 60.23%, SI = 96), which plays a crucial role in maintaining a balance between oxidative stability and cold flow properties of biodiesel. The second largest component is methyl palmitate (RT 15.057 min, 34.83%, SI = 96), which enhances thermal stability and flash point, although it may reduce cold flow performance.

In addition, methyl stearate (RT 17.061 min, 2.27%, SI = 96) was also detected, contributing to increased viscosity and cetane number of the biodiesel. The last key component is methyl myristate (RT 12.994 min, 0.34%, SI = 97), which, despite being

present in a small amount, shows the highest Similarity Index, confirming its strong identification.

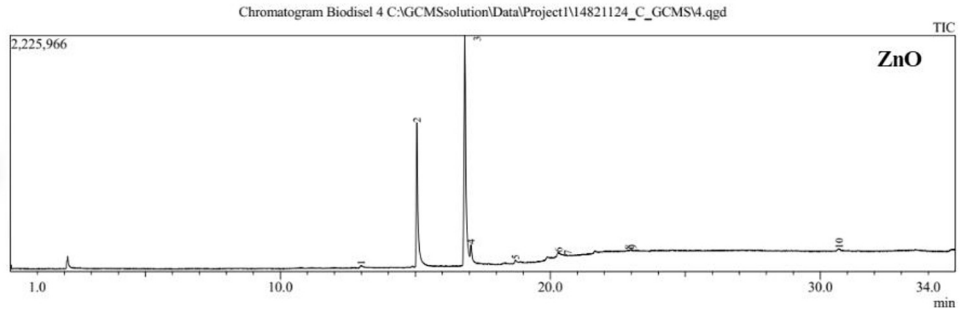

Fig. 7. GC-MS spectra result of ZnO.

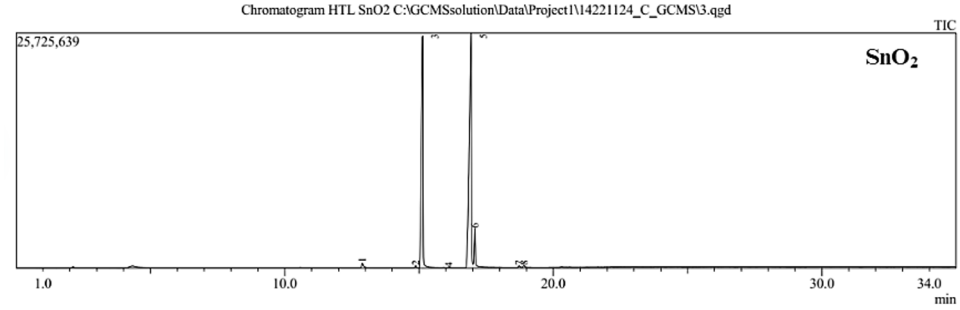

Fig. 8. GC-MS spectra result of SnO_2.

The dominance of methyl oleate and methyl palmitate indicates that biodiesel produced using ZnO catalyst without light has a typical vegetable oil profile, reflecting a balance between saturated and unsaturated fatty acids. This composition confirms that the resulting biodiesel is of high quality, with a high FAME content and chemical characteristics that support its application as a renewable alternative fuel.

GC–MS analysis of the catalyst SnO_2 (Figure 8) without light sample revealed that the biodiesel is dominated by four main compounds with a total content approaching 100%. The most abundant compound is methyl oleate (RT 16.925 min, 55.85%, SI = 96), a methyl ester of oleic acid that plays an important role in providing oxidative stability while maintaining the cold flow properties of biodiesel (**Table 3**). The second major component is methyl palmitate (RT 15.120 min, 37.12%, SI = 96), a methyl ester of palmitic acid that enhances thermal stability and flash point, although it tends to reduce cold flow properties. The next compound is methyl stearate (RT 17.071 min, 4.50%, SI = 96), which contributes to increasing viscosity and improving the cetane number of biodiesel. Lastly, methyl myristate (RT 12.902 min, 0.64%, SI = 97) is present in a small amount but shows the highest identification match. The dominance of methyl oleate and methyl palmitate indicates that the resulting biodiesel achieves a balance between oxidative stability and combustion properties, classifying it as high-quality biodiesel suitable for alternative fuel applications.

Table 3. GC-MS analysis summary.

Catalyst (Without Light)	RT (min)	Compound (Methyl Ester)	%Area	SI (Similarity Index)
SnO_2	16.925	Methyl oleate ($C_{19}H_{36}O_2$)	55.85%	96
	15.120	Methyl palmitate	37.12%	96

		($C_{17}H_{34}O_2$)		
	17.071	Methyl stearate ($C_{19}H_{38}O_2$)	4.50%	96
	12.902	Methyl myristate ($C_{15}H_{30}O_2$)	0.64%	97
FAME			**100%**	–
ZnO	16.836	Methyl oleate ($C_{19}H_{36}O_2$)	60.23%	96
	15.057	Methyl palmitate ($C_{17}H_{34}O_2$)	34.83%	96
	17.061	Methyl stearate ($C_{19}H_{38}O_2$)	2.27%	96
	12.994	Methyl myristate ($C_{15}H_{30}O_2$)	0.34%	97
FAME			**97.34%**	–

4 Conclusions

This study demonstrated that ZnO and SnO_2 catalysts synthesized using roselle flower extract can effectively produce high-quality biodiesel from waste cooking oil. FTIR analysis confirmed the presence of ester groups in biodiesel, with ZnO showing peaks at 1115 cm^{-1} and 1022 cm^{-1}, while SnO_2 exhibited a strong ester carbonyl band at 1744 cm^{-1}, providing clearer evidence of FAME formation. GC–MS analysis revealed that ZnO-catalyzed biodiesel contained 97.34% FAME, dominated by methyl oleate (60.23%) and methyl palmitate (34.83%). In contrast, SnO_2-catalyzed biodiesel achieved nearly 100% FAME, consisting of methyl oleate (55.85%), methyl palmitate (37.12%), with additional contributions from methyl stearate (4.50%) and methyl myristate (0.64%). These results highlight that SnO_2, with a surface area of 51.52 m^2/g, provided significantly higher catalytic performance than ZnO (4.11 m^2/g). Therefore, roselle-extract-based SnO_2 is a promising and eco-friendly heterogeneous catalyst for efficient biodiesel production from waste cooking oil.

References

1. L. R. Kumar, S. K. Yellapu, X. Zhang and R. D. Tyagi, Energy balance for biodiesel production processes using microbial oil and scum. Bioresour. Technol. **272**, 379–388 (2019) https://doi.org/10.1016/j.biortech.2018.10.071
2. D. Singh, D. Sharma, S. L. Soni, S. Sharma, P. Kumar Sharma and A. Jhalani, A review on feedstocks, production processes, and yield for different generations of biodiesel. Fuel. **262**, 116553 (2020) https://doi.org/10.1016/j.fuel.2019.116553
3. B. Panchal, H. M. Kalaji, S. Deshmukh, M. Sharma and W. R. Strobel, Synthesis of methyl esters from silk cotton tree seed kernel oil using dimethyl carbonate and KOH catalysis. Eur. J. Sustain. Dev. Res. **2**, 20 (2018) https://doi.org/10.20897/ejosdr/84899
4. V. Gadore, S. R. Mishra, N. Yadav, G. Yadav and M. Ahmaruzzaman, Metal oxide-based heterogeneous catalysts for biodiesel production. Next Sustain. **2**, 100012 (2023) https://doi.org/10.1016/j.nxsust.2023.100012
5. D.F. Dall'Oglio, M.A.S. Garcia, J.L. Fiorio, W.C. de Abreu, L.N.S. Pereira, A. Braga, E.M. de Moura, A. Guldhe, F. Bux and C.V.R. de Moura, Reusable heterogeneous SnO_2/ZnO catalyst for biodiesel production from acidified/acid oils. J. Braz. Chem. Soc. **32**, 182–193 (2021) https://dx.doi.org/10.21577/0103-5053.20200167
6. C.A. Soto-Robles, P.A. Luque, C.M. Gómez-Gutiérrez, O. Nava, A.R. Vilchis-Nestor, E. Lugo-Medina, R. Ranjithkumar and A. Castro-Beltrán, Study on the effect of the

concentration of Hibiscus sabdariffa extract on the green synthesis of ZnO nanoparticles. Results Phys. **15**, 102807 (2019) https://doi.org/10.1016/j.rinp.2019.102807
7. M. O. Guerrero-Pérez and G. S. Patience, Experimental methods in chemical engineering : Fourier transform infrared spectroscopy—FTIR. Can. J. Chem. Eng. **98**, 25–33 (2020) https://doi.org/10.1002/cjce.23664
8. W. Zhang, F. Liu, F. Liu, C. Huang, H. Zheng, Q. Zhang, Y. Zheng and J. Gao, Microstructural evolution and cracking behavior of Hastelloy X superalloy fabricated by laser directed energy deposition. J. Alloys Comp. **5**, 164179 (2022) https://doi.org/10.1016/j.jallcom.2022.164179
9. E. Q. González, E. L. Medina, R. V. Q. Robles, H. E. G. Gálvez, Y. A. B. Lopez, E. V. Viveros, F. A. Molina, A. R. V. Nestor, P. A. L. Morales. A study of the optical and structural properties of SnO_2 nanoparticles synthesized with Tilia cordata applied in methylene blue degradation. Symmetry, **14(11)**, 2231 (2022). https://doi.org/10.3390/sym14112231
10. S. Fatimah, R. Ragadhita, D. F. Al Husaeni, and A. B. D. Nandiyanto, How to calculate crystallite size from X-ray diffraction (XRD) using Scherrer method. ASEAN J. Sci. Eng. **2**, 65–76 (2022) https://doi.org/10.17509/ajse.v2i1.37647
11. N. Aggarwal, H. Kaur, N. Kumar, J. Kaur, S. Malhotra, A. Sharma, S. Tripathi, R. S. Panwar, P. Patial. Evaluation of photocatalytic efficacy of biosynthesized tetragonal SnO_2 nanoparticles. Results Chem., **5**, 100803 (2023). https://doi.org/10.1016/j.rechem.2023.100803
12. Y. Sivarajan, K. A. Ishak, J.S. Yaacob. Green synthesis of tin oxide (SnO_2) nanoparticles using ginger extracts for photocatalytic degradation of organic dyes in wastewater. Appl. Biochem. Biotechnol. **197(9)**, 5668–5693 (2025) https://doi.org/10.1007/s12010-025-05293-2
13. D. Aviliani, F. I. P. Sari, and R. G. Mahardika, The effectiveness of Pandan sea (Pandanus tectorius) cellulose active charcoal in reducing BOD, COD, TSS levels in liquid waste tapioca. Stannum J. Sains dan Terap. Kim. **4**, 52–59 (2022). https://doi.org/10.33019/jstk.v4i2.3326
14. M. Thommes, K. Kaneko, A.V. Neimark, J.P. Olivier, F. Rodriguez-Reinoso, J. Rouquerol and K.S.W. Sing, Physisorption of gases, with special reference to the evaluation of surface area and pore size distribution (IUPAC technical report). Pure App. Chem. **87**, 1051-1069 (2015). https://doi.org/10.1515/pac-2014-1117
15. J.I. Goldstein, D.E. Newbury, J.R. Michael, N.W.M. Ritchie, J.H.J. Scott and D.C. Joy, Scanning electron microscopy and X-ray microanalysis (Spinger, 2018)